A tunable metal oxide shell as a spacer to study energy transfer in semiconductor nanocrystals

Anna Loiudice[†], Seryio Saris[†], Raffaella Buonsanti[†]*

[†]Laboratory of Nanochemistry for Energy (LNCE), Institute of Chemical Sciences and Engineering (ISIC), École Polytechnique Fédérale de Lausanne, Rue de l'Industrie 17, 1950 Sion, Valais, Switzerland.

ABSTRACT: Colloidal semiconductor nanocrystals (NCs) are promising components in various optoelectronic and photocatalytic devices, but the mechanism of energy transport in these materials remains to be further understood. Here, we investigate the distance-dependence of the electronic interactions between $CsPbBr_3$ cubes and CdSe nanoplateles using an alumina (AlO_x) shell as a spacer. $CsPbBr_3$@AlO_x core@shell NCs are synthesized via colloidal atomic layer deposition (c-ALD), which allows to fine tune the oxide thickness and, thus, the distance *d* between the two NCs. This versatile material platform shows that the electronic interactions between the $CsPbBr_3$ NCs and the CdSe NPLs can be tuned from electron to energy transfer by increasing the shell thickness, while previous studies on the same system had been limited only to electron transfer. Considering the applicability of the c-ALD to different NCs, we suggest that metal oxide shells spacers synthesized by this approach can generally be used to study energy transfer mechanisms at the nanoscale.

KEYWORDS: metal oxide shell, semiconductor nanocrystals, hybrid nanomaterials, perovskites, FRET, nanoscale energy transport

The unique size- and shape- dependent optical properties of semiconductor nanocrystals (NCs) offer exciting opportunities for controlling the energy transfer at the nanoscale, thus motivating research towards next-generation optoelectronic devices (i.e. light emitting diodes, solar cells, luminescent solar concentrators) and biomedical

applications that implement imaging, sensing and labeling with semiconductor NCs.[1-5] In all these technologies, the electronic interactions among NCs must be evaluated and possibly engineered to achieve optimal performance.[6-8]

Depending on the application of interest, electron transfer (ET) of the generated excitons or Förster resonance energy transfer (FRET) might be more or less desirable. In particular, ET is preferable for those devices which benefit from photoinduced charge separation, such as for photodetectors and solar cells. Compared to charge transfer processes, FRET is particularly appealing because it allows the transport of charge-neutral excitons between NCs despite the presence of the insulating surface ligands.[9-11] Light emitting diodes would particularly benefit from FRET in semiconductor NC films.[12]

FRET has been demonstrated in artificially engineered structures with graded band gap mostly based on CdSe, CdTe and PbS NCs.[13-15] In one example, a cascade-like energy transfer across ascending diameter QDs layers was used to enhance the infrared-range emission of PbS solids.[13] However, FRET-based devices are still limited by the poor efficiencies and slow kinetics of the process. As evidenced by recent findings regarding dimensionality effects on FRET,[16] fundamental studies on a broader selection of systems (i.e. different surface chemistries, compositions and shapes) are needed to understand and to overcome the limiting factors so to fully exploit the potential of energy transfer in semiconductor NCs. In this scenario, NC distance-dependent measurements would be key to gain further insights into the transfer processes that occur in different binary NC mixtures. Unfortunately, the conventional ligand exchange strategies used so far to control the NC distance are not universal as they cannot be easily translated to systems with challenging surface chemistry and/or with poor stability, such as the recently emerged perovskite NCs to cite one example.[17-20]

Herein, we propose to use an oxide shell with tunable thickness to investigate the distance-dependence of the energy transfer between $CsPbBr_3$ NCs and CdSe nanoplateles (NPLs).

All-inorganic perovskite NCs, namely $CsPbX_3$ (X=Br, I, Cl), have recently emerged as a class of semiconductors showcasing outstanding optoelectronic properties.[21,22] Due to their large polarizability and absorption cross-section, near-unity quantum yields, and small Stokes shifts, perovskite NCs are envisioned to be excellent FRET donors.[21,22] Yet, energy transfer studies are mostly limited to homo-FRET among

perovskite NCs with the same composition and hetero-FRET between perovskite NCs and molecular dyes.[23-26]

Recently, the electronic interactions between $CsPbBr_3$ and CdSe NCs with different sizes and shapes were investigated.[27,28] CdSe is an ideal system to use as an acceptor thanks to the synthetic flexibility achieved so far for these NCs, which implies an impressive tunability of its optoelectronic properties. While the basic requirements for FRET to occur in this system were satisfied (i.e. the overlap between the donor emission and acceptor absorption), no appreciable FRET was detected and ET was proposed as the only pathway for the charge transport.[27]

Building on our recent developments on colloidal atomic layer deposition (c-ALD)[29], we use an amorphous shell of alumina (AlO_x) as a tunable spacer between $CsPbBr_3$ NCs and CdSe NPLs. CdSe NPLs were chosen as the acceptor because of the above-mentioned dimensionality effects, which were recently reported.[16]

This approach allowed us to study the distance dependence of the electronic interactions in this NC system and to demonstrate that FRET becomes the dominant mechanism between $CsPbBr_3$@AlO_x donors and CdSe NPL acceptors for shell thicknesses above 2.5 nm, corresponding to a center-to-center distance of around 10 nm.

The $CsPbBr_3$ and the CdSe NPLs were prepared according to published procedures.[29,16] **Figure 1** reports the transmission electron microscopy (TEM) images of highly monodisperse $CsPbBr_3$ NCs with cubic shape and edge size of 7.6 nm (Figure 1a) and 5-monolayer (ML) CdSe NPLs with lateral dimensions 3.9 nm x 16.3 nm (Figure 1b and Figure S1). Satisfying a basic requirement for FRET to occur, the $CsPbBr_3$ NC donors exhibit an emission peak that overlaps with the absorption of 5-ML CdSe NPL acceptors (Figure 1c).

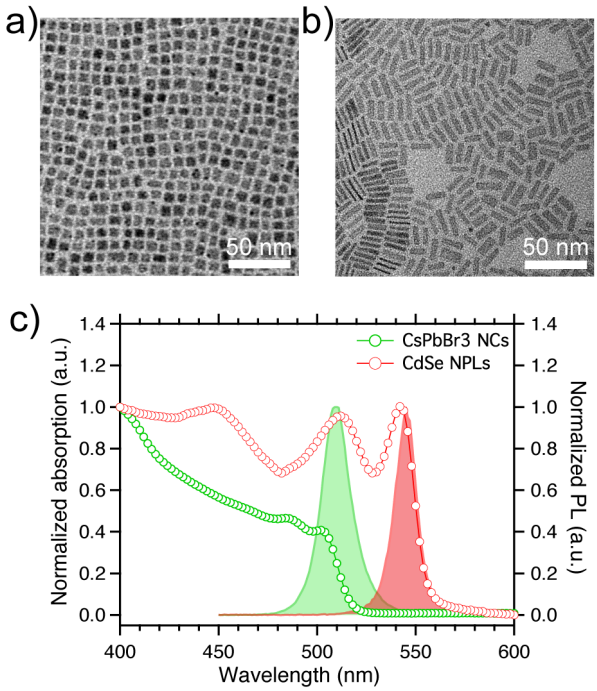

Figure 1 (a,b) TEM images of the as-synthesized $CsPbBr_3$ NCs and CdSe NPLs and (c) corresponding normalized UV-Vis absorption (scatter line) and photoluminescence (continuous line) spectra acquired in solution.

To study the distance dependence of the electronic interactions between $CsPbBr_3$ NCs and CdSe NPLs, we grew an alumina shell around the $CsPbBr_3$ NCs by using our recently developed c-ALD in solution to form $CsPbBr_3@AlO_x$ NCs (Figure S2) and we tuned its thickness from 1 nm to 10 nm using different ALD cycles.[29]

We evaluated the shell thickness by combining grazing incidence small angle X-ray scattering (GISAXS) measurements and dynamic light scattering (DLS) in solution (Figures S3). The values obtained by the two techniques were in excellent agreement with each other, thus providing a solid support to the quantification of the donor-acceptor spacing that will be used for later analysis.

The as-prepared $CsPbBr_3@AlO_x$ donors (D) were dispersed in hexane and mixed with CdSe NPL acceptors (A) to form binary mixtures in controlled ratios of concentrations (i.e. particle number, see SI for details) and then drop-casted on glass substrates where the solvent rapidly evaporated. **Figure 2**a reports the TEM images of two representative mixtures, one at 50D:50A ratio and the other at 75D:25A ratio. The images evidence substantive regions where $CsPbBr_3@AlO_x$ NCs and CdSe NPLs are homogenously mixed. At lower donor concentration the CdSe NPLs tend to assembly and to stack vertically. The overall D:A assembly remains very much alike when $CsPbBr_3@AlO_x$

NCs with different shell thicknesses are utilized as donors, which gives us confidence regarding the distance-dependent trends described below.

When two NCs are in close vicinity both ET and FRET may take place. In our system, Figure 1c illustrates that the requirements for FRET to occur are satisfied in the chosen binary system. At the same time, because the conduction band of the $CsPbBr_3$ NCs is positioned at higher energy respect to the one of CdSe NCs (by around 50-100 meV), ET is equally possible.[30,31] To gain insights into the dominating process, we investigated the photoluminescence (PL) of the D:A mixtures with different ratios and shell thicknesses. The steady-state PL measurements evidence quenching of the donor PL in all the binary mixtures (Figure S4). The higher the donor concentration is, the lower the PL quenching is, which is in agreement with a decreased probability to find an acceptor in the close vicinity of a donor. This observation indicates that electronic transfer occurs between the $CsPbBr_3@AlO_x$ NCs and the CdSe NPLs but does not allow to distinguish between ET and FRET. Photoluminescence excitation (PLE) measurements on binary mixture films of $CsPbBr_3@AlO_x$ NCs with an average shell thickness of 3.6 nm and CdSe NPLs at different ratios were performed to learn more about process involved (Figure 2b). The PLE spectra were collected at 570 nm to be as far as possible from the emission tail of the $CsPbBr_3$ donor. The data show that, for all the mixtures, the spectral features of both the donor and the acceptor are present, which is consistent with FRET. When no AlO_x shell is present and only the native ligands separate the two NCs, direct ET is favored (Figure S5). As the shell thickness increases, more pronounced features of the donors appear in the PLE spectra indicating an increasingly predominant FRET over ET (Figure S5).

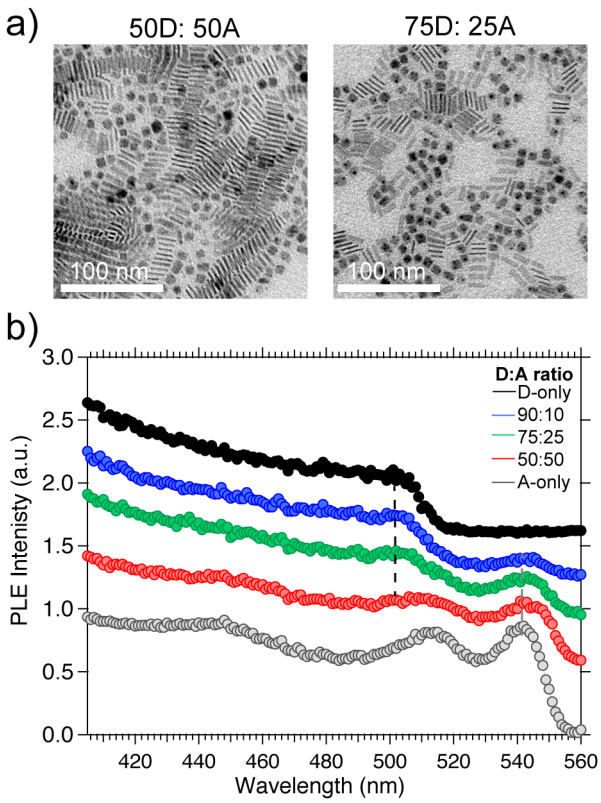

Figure 2 a) TEM images of $CsPbBr_3@AlO_x$ mixed with CdSe NPLs at 50D:50A (left) and 75D:25A (right) ratios; b) PLE spectra (vertically offset for clarity) collected at 570 nm for films at various D:A for an AlO_x shell of 3.6 nm thick. The gray and purple curves are the PLE spectra for the A-only and D-only films. The dashed lines indicate the position of the maximum for the donor (black dashed line) and acceptor (gray dashed lines).

Next, transient spectroscopy measurements were performed to eventually provide a more quantitative interpretation of the results. **Figure 3**a,b show representative time and energy resolved photoluminescence intensity maps for binary mixture films at a fixed composition (50D:50A) for short (Figure 3a, 2.4 nm) and long (Figure 3b, 4.7 nm) D-A distances. It is clear that the donor lifetime is longer in the latter. We slide the intensity maps to extract a more detailed picture on these two samples, which we compare with the A-only and D-only samples (Figure 3c). For all samples, we report the PL spectra at shorter (0-10ns) and longer (80-95ns) times. First, we note that the PL decay is more pronounced in the mixture than the donor-only samples. Second, at longer times the PL peak of the donor is still visible in the mixture with the larger D-A distance while it is already completely quenched in the mixture with the smaller D-A distance (Figure 3c).

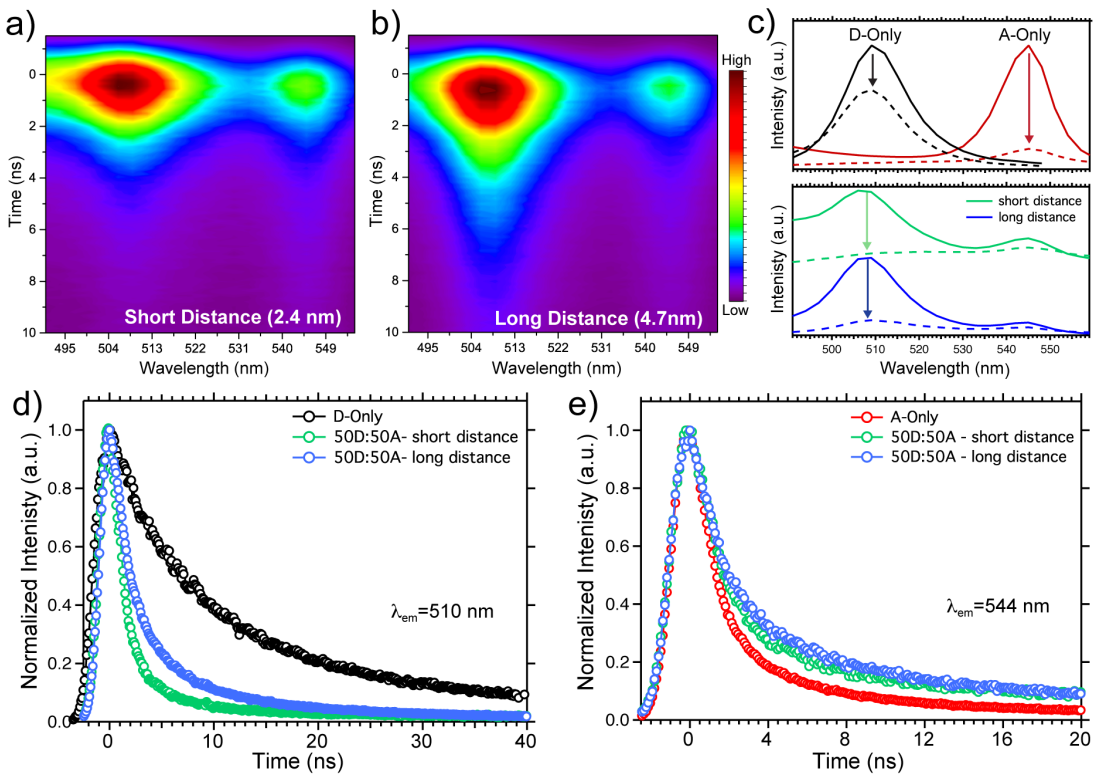

Figure 3 a-b) Time- and energy-resolved photoluminescence intensity maps for short distance (2.4 nm) and long distance (4.7 nm) in equimolar binary mixtures containing both spectral information and decay dynamics. c) Spectra from early and late time windows 0-10 ns (solid line) and 80-95 ns (dashed line) for the neat donor and acceptor (top) and for the 50% binary mixture at long and short distances. d,e) Decay dynamics of the features centered at 510 nm and 544 nm respectively, comparing the decay dynamics of the neat donor and acceptor with the one in the binary mixture at short and long distances.

Additional informations can be extracted by comparing the decay dynamics of the donor and acceptor in the mixed films with the ones of D-only and A-only films. A marked decrease in the radiative lifetime of the donor (Figure 3d) and an increase of the radiative acceptor lifetime (Figure 3e) are evident in the mixed film compared to the neat films. We also compare the lifetime decay for short and long distances observing a reduction in the lifetime for the mixed film with donor and acceptor at shorter distance. It must be noted that the increase in the acceptor lifetime is smaller compared to the decrease in donor lifetime (see Figure 3d,e and Figure S6), which suggest that both ET and FRET are contributing to the donor quenching. Likewise, the acceptor lifetime increase is higher for the longer distances in agreement with the PLE data (Figure S5). This suggests that for this system, ET is a faster process respect to FRET, and when ET is present (short NC-NC distances), FRET is absent or negligible. Thus, precisely tuning of the AlO_x shell thickness allows suppressing one process respect to the other in function of the desired application.

To quantify the observed differences in the transfer dynamics when changing the D-A distance, the energy transfer rates (K_{ET}) were calculated from the averaged lifetime of the donor in the mixtures and in the neat sample and are plotted versus the corresponding D-A distances in **Figure 4** (see also Table S1, Figure S7 and details in the SI). As the distance decreases the energy transfer becomes progressively faster. Indeed, the averaged measured K_{ET} increases from 0.01 ns^{-1} to 0.1 ns^{-1} upon decreasing the average center-to-center distance from 17.3 nm to 9.8 nm showing a 10-fold increase in the K_{ET} for shorter distances.

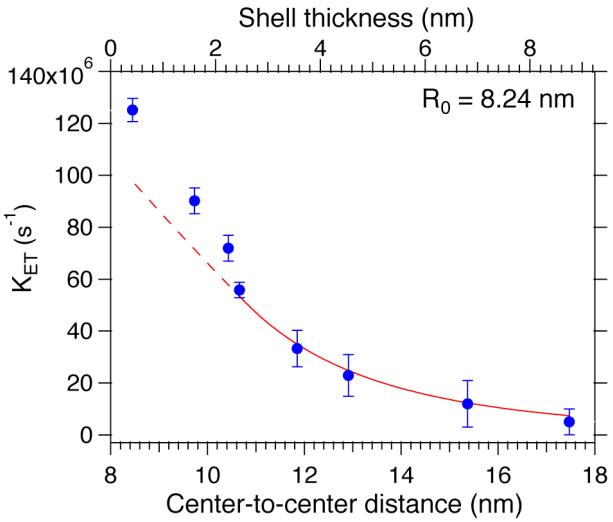

Figure 4 Energy transfer rates (k_{ET}) vs. the center-to-center distance (d) calculated for the different AlO_x shell thicknesses. The red line is the fit of the data for d >10 nm (R_0=8.24 nm, n=4).

K_{ET} is defined by the following equation:

$$K_{ET} = \frac{1}{\tau_D}\left(\frac{R_0}{d}\right)^n$$

where τ_D is the donor lifetime, d is the center-to-center distance between the donor and the acceptor, R_0 is the Förster radius defined as the distance at which the efficiency is 50% and n is the exponent indicating the dependence of FRET rate on the distance. n is typically 6 for a pair of point-like donor and acceptor and is 4 for higher acceptor dimensionalities, which is likely the case for NC films.[11] The data in Figure 4 were fitted by this equation to estimate the Förster radius as well as to evaluate the distance dependence trend. By excluding the data point for d < 10 nm, we found that the best fit is indeed obtained for n=4 which suggests that FRET becomes the main mechanism of exciton transfer in this system for longer distance (additional discussion in SI and

Figure S5,S6). We obtained that R_0 is equal to 8.2 nm, which is in the same size range of other previously reported radii in NC mixed films.[32]

In conclusion, we have introduced a hybrid material platform wherein an oxide shell with tunable thickness allows to perform careful distance-dependent studies on the transfer of excitonic energy in semiconductor NC films. This approach allowed us to define the electronic interactions at different distances in the $CsPbBr_3$ NCs/CdSe NPLs binary system. The finding that energy transfer can take place for this highly emissive donors unlocks the opportunity of new operation motifs for devices such as lasers and light emitting diodes.[12] Future studies will be directed to increase the transfer efficiencies and improve the kinetics by further exploring dimensionalities effects (i.e. $CsPbBr_3$ NPLs/CdSe@AlO_x NPLs, Figure S8). Initial results reveal that FRET can be then be used to drive photoelectrochemical reactions with increased photocurrents compared to D-only and A-only films, in addition to provide improved stability (Figure S9). Considering the applicability of the c-ALD to different NCs, we suggest that metal oxide shells spacers synthesized by this approach can generally be used to study energy transfer mechanisms at the nanoscale.

Methods.

Materials: All chemicals were purchased from Sigma Aldrich and used without purification, unless specified: cesium carbonate (Cs_2CO_3, 99.9%), lead(II) bromide ($PbBr_2$, 99.99%, Alfa Aesar), oleic acid (OLAC, technical grade, 90%), oleylamine (OLAM, technical grade, 70%), 1-octadecene (ODE, technical grade, 90%), octane (anhydrous, ≥99%), methyl acetate (MeOAc, anhydrous, 99.5%), Selenium powder (Se, 99.5% trace metals), Cadmium acetate hydrate ($Cd(Ac)_2$, 99.99%), and trimethylaluminum (TMA, 98%, Strem).

The NCs used in this work were synthesized by using slightly modified syntheses from the literature.[16,33] Specific details follow.

$CsPbBr_3$ NCs: $PbBr_2$ (0.21 g) and ODE (15 mL) were stirred in a 50 mL round-bottom flask and degassed under vacuum at 120 °C for 1 h. The flask was then filled with N_2 and kept under constant N_2 flow. OLAC and OLAM (1.5 mL each) were injected, and the mixture was kept at this temperature until all the $PbBr_2$ was dissolved. The temperature was then increased to 165 °C. The Cs-OLA (1.2 mL) precursor, preheated to 100 °C under N_2 atmosphere, was swiftly injected into the reaction mixture. The

reaction mixture turned yellow, and the reaction was quenched by immediate immersion of the flask into an ice bath (~5 s after injection). The synthesized NCs were precipitated by centrifugation at 6000 rpm for 30 min, the supernatant was removed, and the NCs were re-dissolved in 1.5 mL of hexane. A second wash was carried out by adding ethyl acetate in a 1:1 ratio with hexane, the mixture was centrifuged, and the precipitate was dissolved in octane, giving a final concentration of ~10 mg/mL.

CdSe NPLs: Cd(myristate)$_2$ was synthesized according to reported procedure.[16] 170 mg of Cd(myristate)$_2$ and 14 ml of ODE were degassed for 30min at room temperature in a three neck-flask. Then under N_2 the flask was heated to 240ºC. Meanwhile, 12 mg of Se powder was sonicated in 1ml ODE for 5min. At 240ºC the Se solution was quickly injected in the reaction mixture and after 20 seconds (the solution became dark orange), 60mg of Cd(Ac)$_2$ was introduced. The reaction mixture was kept at 240ºC for 10 min and then was cooled down with to 150ºC with air-flow, and allowed to slowly cool down further. At 70ºC, 2 ml of OLAC in 10 ml of hexane were added to the reaction flask. The mixture was taken to the glove box to carry out the washing procedure, which consist in centrifugation and redeseprsion in hexane. Please note that a little percentage of spherical CdSe NCs may be present together with the CdSe NPLs that were removed through size selective precipitation.

$CsPbBr_3$@AlO_x with different AlO_x thickness: In a three-necked flask, a solution of $CsPbBr_3$ NCs in octane (typically 150 µL of a 5 mM solution in octane) was gently stirred under N_2 flow. An additional amount of octane (typically 2 mL) was added to ensure a good dispersion so to guarantee a homogeneous growth of the shell. One c-ALD cycle consists of (1) dropwise addition (1 mL/h) of TMA diluted in octane to the NC solution; (2) 5 min waiting time to ensure that the reaction in step 1 was completed; (3) addition of O_2 gas by mean of a mass flow controller; and (4) 5 min waiting time. This cycle is repeated n times to reach the desired thickness. 80 µL from a diluted TMA solution in octane with a concentration of 0.4×10^{-3} µM were added each cycle. Some minimal adjustment might be needed from batch to batch. The full process was automated by using a custom-made Lab-View program where precursor amount, injection speed, and waiting time are independently defined. In order to retain the colloidal stability in the organic solvent of the as-synthesized core@shell NCs, OLAC was introduced in place of TMA after 8-10 cycles. This step functionalizes the surface of the shell, which can continue to grow without any precipitation of the NCs.

$CsPbBr_3@AlO_x$ NCs with different shell thickness were synthesized ranging from 1.5 to 10 nm thick. Additional details on the c-ALD procedure can be found in ref 27.

Electron Microscopy: Transmission electron microscopy (TEM) images were acquired on an FEI Tecnai-Spirit at 120 kV. High-angle annular dark-field scanning TEM (HAADF-STEM) images were acquired on an FEI Tecnai-Osiris at 200 kV.

Film preparation: $CsPbBr_3@AlO_x$ NCs with different shell thickness were mixed with CdSe NPLs in hexane at the desired molar ratio. See SI for detail on NC mixture films preparation. 10ul of the mixture was drop casted at the center of a glass substrate with a size of 2.5x2.5 cm^2.

Optical Spectroscopy: All optical measurements, including photoluminescence (PL) emission spectra, Photoluminescence Excitation (PLE), and time-resolved fluorescence lifetimes (TRPL) were collected on a Horiba Jobin Yvon Fluorolog-3 instrument with a photomultiplier tube (PMT) as detector. For the TRPL the excitation source is a Horiba nanoLED-370 with an excitation wavelength of 369 nm, a pulse duration of 1.3 ns, and a repetition rate of 100 kHz. All the measurements were performed under N_2 by using a customized cell.

AUTHOR INFORMATIONS

Corresponding author

*E-mail: raffaella.buonsanti@epfl.ch

Author Contributions

A.L and R.B. conceived the work. A.L. performed all the described experiments from the synthesis to the spectroscopic measurements. S.S. contributed to the discussion and analysis of the data. The manuscript was written through contributions of all authors. All authors have given approval to the final version of the manuscript.

Notes

The authors declare no competing financial interest.

ACKNOWLEDGMENTS

S.S. acknowledges the Swiss National Science Foundation (AP Energy Grant, project number PYAPP2_166897/1) for financial support. The GISAXS experiments were

performed on the beamline ID10 at the European Synchrotron Radiation Facility (ESRF), Grenoble, France (proposal number MA- 4141). We are grateful to Dr. Oleg Konovalov and Dr. Andrei Chumakov at ESRF for helpful discussions on the GISAXS data analysis.

REFERENCES

[1] Konstantatos, G.; Howard, I.; Fischer, A.; Hoogland, S.; Clifford, J.; Klem, E.; Levina, L.; Sargent, E.H. Ultrasensitive solution-cast quantum dot photodetectors. *Nature*, **2006**, 442, 180-183.
[2] Bae, W.K.; Kwak, J.; Lim, J.; Lee, D.; Nam, M.K.; Char, K.; Lee, C.; Lee, S. Multicolored Light-Emitting Diodes Based on All-Quantum-Dot Multilayer Films Using Layer-by-Layer Assembly Method. *Nano Lett.* **2010**, 10, 7, 2368-2373.
[3] Chuang, C.-H. M.; Brown, P.R.; Bulović, V.; Bawendi, M.G. Improved performance and stability in quantum dot solar cells through band alignment engineering. *Nature Materials*, **2014**, 13, 796-801.
[4] Bruchez, M. J.; Moronne, M.; Gin, P.; Weiss, S.; Alivisatos, A.P. Semiconductor nanocrystals as fluorescent biological labels. *Science*, **1998**, 281, 2013-2016.
[5] Medintz, I.L.; Uyeda, H.T.; Goldman, E.R.; Mattoussi, H. Quantum dot bioconjugates for imaging, labelling and sensing. *Nature Materials*, **2005**, 4, 435-446.
[6] Kagan, C.R.; Murray, C.B. Charge transport in strongly coupled quantum dot solids. *Nat. Nanotech.* **2015**, 10, 1013-1026.
[7] Talapin, D.V.; Lee, J.-S.; Kovalenko, M.V.; Shevchenko, E.V. Prospects of Colloidal Nanocrystals for Electronic and Optoelectronic Applications. *Chem. Rev.* **2010**, 110, 389-458.
[8] Guyot-Sionnest, P. Electrical Transport in Colloidal Quantum Dot Films. *J. Phys. Chem. Lett.* **2012**, 3, 1169-1175.
[9] Achermann, M.; Petruska, M.A.; Kos, S.; Smith, D.L.; Koleske, D.D.; Klimov, V.I. Energy-transfer pumping of semiconductor nanocrystals using an epitaxial quantum well. *Nature*, **2004**, 429, 642-646.
[10] Anikeeva, P.O.; Halpert, J.E.; Bawendi, M.G.; Bulović, V. Electroluminescence from a Mixed Red−Green−Blue Colloidal Quantum Dot Monolayer. *Nano Lett.*, **2007**, 7, 2196-2200.
[11] Rogach, A.L.; Klar, T.A.; Lupton, J.M.; Meijerink, A.; Feldmann, J. Energy transfer with semiconductor nanocrystals. *J. Mater. Chem.*, **2009**, 19, 1208-1221.
[12] Moroz, P.; Romero, L.R.; Zamkov, M. Colloidal semiconductor nanocrystals in energy transfer reactions. *Chem. Commun.*, **2019**, 55, 3033-3048.
[13] Xu, F.; Ma, X.; Haughn, C.R.; Benavides, J.; Doty, M.F.; Cloutier, S.G. Efficient Exciton Funneling in Cascaded PbS Quantum Dot Superstructures. *ACS Nano*, **2011**, 5, 9950-9957.
[14] Crooker, S.A.; Hollingsworth, J.A.; Tretiak, S.; Klimov, V.I. Spectrally Resolved Dynamics of Energy Transfer in Quantum-Dot Assemblies: Towards Engineered Energy Flows in Artificial Materials. *Phys. Rev. Lett.*, **2002**, 89, 186802-18606.
[15] Franzl, T.; Klar, T. A.; Schietinger, S.; Rogach, A. L.; Feldmann, J. Exciton Recycling in Graded Gap Nanocrystal Structures. *Nano Lett.*, **2004**, 9, 1599-1603.
[16] Rowland, C.E.; Fedin, I.; Zhang, H.; Gray, S.K.; Govorov, A.O.; Talapin, D.V.; Schaller, R.D. Picosecond energy transfer and multiexciton transfer outpaces Auger recombination in binary CdSe nanoplatelet solids. *Nature Materials* **2015**, 14, 484–489.
[17] Akselrod, G.M.; Prins, F.; Poulikakos, L.V.; Lee, E.M.Y.; Weidma, M.C.; Mork, A.J.; Willard, A.P.; Bulović, V.; Tisdale, W.A. Subdiffusive Exciton Transport in Quantum Dot Solids. *Nano Lett.*, **2014**, 14, 3556-3562.

[18] Wang, C.; Weiss, E.A. Accelerating FRET between Near-Infrared Emitting Quantum Dots Using a Molecular J-Aggregate as an Exciton Bridge. *Nano Lett.*, **2017**, 17, 5666-5671.
[19] Kodaimati, M.S.; Wang, C.; Chapman, C.; Schatz, G.C.; Weiss, E.A. Distance-Dependence of Interparticle Energy Transfer in the Near-Infrared within Electrostatic Assemblies of PbS Quantum Dots. *ACS Nano*, **2017**, 11, 5041-5050.
[20] Melle, S.; Calderoń, O.G.; Laurenti, M.; Mendez-Gonzalez, D.; Egatz-Gomez, A.; Lopez-Cabarcos, E.; Cabrera-Granado, E.; Día, E.; Rubio-Retama, J. Förster Resonance Energy Transfer Distance Dependence from Upconverting Nanoparticles to Quantum Dots. *J. Phys. Chem. C*, **2018**, 122, 18751-18758.
[21] Akkerman, Q.A.; Rainò, G.; Kovalenko, M.V.; Manna, L. Genesis, challenges and opportunities for colloidal lead halide perovskite nanocrystals. *Nature Materials*, **2018**, 17, 394–405.
[22] Kovalenko, M.V.; Protesescu, L.; Bodnarchuk, M.I. Properties and potential optoelectronic applications of lead halide perovskite nanocrystals. *Science*, **2017**, 358, 745-750.
[23] de Weerd, C.; Gomez, L.; Zhang, H.; Buma, W.J.; Nedelcu, G.; Kovalenko, M.V.; Gregorkiewic, T. Energy Transfer between Inorganic Perovskite Nanocrystals. *J. Phys. Chem. C*, **2016**, 120, 13310-13315.
[24] Bouduban, M.E.F.; Burgos-Caminal, A.; Ossola, R.; Teuscher, J.; Moser, J.E. Energy and charge transfer cascade in methylammonium lead bromide perovskite nanoparticle aggregates. *Chem. Sci.*, **2017**, 8, 4371-4380.
[25] Hofmann, F.J.; Bodnarchuk, M.I.; Protesescu, L.; Kovalenko, M.V.; Lupton, J.M.; Vogelsang, J. Exciton Gating and Triplet Deshelving in Single Dye Molecules Excited by Perovskite Nanocrystal FRET Antennae. *J. Phys. Chem. Lett.*, **2019**, 10, 1055-1062.
[26] Hofmann, F.J.; Bodnarchuk, M.I.; Dirin, D.N.; Vogelsang, J.; Kovalenko, M.V.; Lupton, J.M. Energy Transfer from Perovskite Nanocrystals to Dye Molecules Does Not Occur by FRET. *Nano Lett.*, **2019**, 19, 8896-8902.
[27] Brumberg, A.; Diroll, B.T.; Nedelcu, G.; Sykes, M.E.; Liu, Y.; Harvey, S.M.; Wasielewski, M.R.; Kovalenko, M.V.; Schaller, R.D. Material Dimensionality Effects on Electron Transfer Rates Between CsPbBr3 and CdSe Nanoparticles. *Nano Lett.*, **2018**, 18, 4771-4776.
[28] Dey, S.; Cohen. H.; Pinkas, I.; Lin, H.; Kazes, M.; Oron, D. Band alignment and charge transfer in CsPbBr3–CdSe nanoplatelet hybrids coupled by molecular linkers. *J. Chem. Phys.*, **2019**, *151*, 174704-174713.
[29] Loiudice, A.; Strach, M.; Saris, S.; Chernyshov, D.; Buonsanti, R. Universal Oxide Shell Growth Enables in Situ Structural Studies of Perovskite Nanocrystals during the Anion Exchange Reaction. *J. Am. Chem. Soc.* **2019**, *141*, 8254-8263.
[30] Ravi, V. K.; Markad, G. B.; Nag, A. x Band Edge Energies and Excitonic Transition Probabilities of Colloidal CsPbX3 (X = Cl, Br, I) Perovskite Nanocrystals. *ACS Energy Lett*., **2016**, *1*, 665−671.
[31] Li, Q.; Lian, T. Area- and Thickness-Dependent Biexciton Auger Recombination in Colloidal CdSe Nanoplatelets: Breaking the "Universal Volume Scaling Law". *Nano Lett.*, **2017**, *17*, 3152−3158.
[32] Mork, A.J.; Weidman, M.C.; Prins, F.; Tisdale, W.A. Magnitude of the Förster Radius in Colloidal Quantum Dot Solids. *J. Phys. Chem. C* **2014**, 118, 13920-13928.
[33] Protesescu, L.; Yakunin, S.; Bodnarchuk, M. I.; Krieg, F.; Caputo, R.; Hendon, C.; Yang, R. X.; Walsh, A.; Kovalenko, M. V. Nanocrystals of Cesium Lead Halide Perovskites (CsPbX3, X = Cl, Br, and I): Novel Optoelectronic Materials Showing Bright Emission with Wide Color Gamut. *Nano Lett.* ***2015***, 15, 3692-3696.